HHS Public Access

Author manuscript

Sci Transl Med. Author manuscript; available in PMC 2023 February 28.

Published in final edited form as:

Sci Transl Med. 2022 April 20; 14(641): eabe9726. doi:10.1126/scitranslmed.abe9726.

In utero exposure to maternal anti–aquaporin-4 antibodies alters brain vasculature and neural dynamics in male mouse offspring

Simone Mader[1,2,*,†], **Lior Brimberg**[1,†], **An Vo**[1], **Joshua J. Strohl**[1,3], **James M. Crawford**[4], **Alexandre Bonnin**[5], **Joseph Carrión**[1], **Delcora Campbell**[1], **Tomás S. Huerta**[1,3], **Andrea La Bella**[1], **Roseann Berlin**[1], **Stephen L. Dewey**[1], **Matthew Hellman**[1], **David Eidelberg**[1], **Irena Dujmovic**[6,7], **Jelena Drulovic**[6], **Jeffrey L. Bennett**[8], **Bruce T. Volpe**[1], **Patricio T. Huerta**[1,3], **Betty Diamond**[1]

[1]The Feinstein Institutes for Medical Research, Northwell Health, Manhasset NY 11030, USA.

[2]Institute of Clinical Neuroimmunology, Biomedical Center of the Ludwig Maximilian University of Munich, Munich 82152, Germany.

[3]Department of Molecular Medicine, Zucker School of Medicine at Hofstra/Northwell, Manhasset, NY 11030, USA.

[4]Department of Pathology and Laboratory Medicine, Northwell Health, Manhasset, NY 11030, USA.

[5]Department of Physiology and Neurosciences, Zilkha Neurogenetic Institute, University of Southern California, Keck School of Medicine, Los Angeles, CA 90033, USA.

[6]Clinical Center of Serbia University School of Medicine, Belgrade, 11000, Serbia.

[7]Department of Neurology, University of North Carolina, School of Medicine, Chapel Hill, NC 27517, USA.

[8]Department of Neurology and Ophthalmology, Programs in Neuroscience and Immunology, University of Colorado Denver, School of Medicine, Denver, CO 80045, USA.

[*]Corresponding author simone.mader@med.uni-muenchen.de.
[†]These authors contributed equally to this work.

Author contributions: S.M. designed and performed experiments involving immunohistology of embryonic and adult brains, qPCR, site-directed mutagenesis, Western blot, mouse behavior, microPET, cell-based assay, brain deglycosylation, and enzyme-linked immunosorbent assay (ELISA); performed statistical analysis; prepared figures; and wrote the manuscript. L.B. designed and performed experiments involving immunohistology of embryonic and adult brains, qPCR, mouse behavior, in situ hybridization; performed statistical analysis; prepared figures; and wrote the manuscript. A.V. and D.E. designed experiments involving microPET, analyzed the microPET data, prepared figures, and contributed to manuscript preparation. J.C., S.L.D., and M.H. designed and conducted experiments involving microPET and contributed to manuscript preparation. J.J.S. performed experiments involving mouse behavior and neuronal recordings and contributed in the preparation of figures and the manuscript. J.M.C. and A.B. designed and analyzed the experiments involving placenta pathology and contributed in the preparation of the manuscript. D.C. designed and performed experiments involving immunohistology of brains and in situ hybridization and contributed in the preparation of the manuscript. T.S.H. and A.L.B. contributed in experiments involving mouse behavior and contributed in the preparation of figures and the manuscript. R.B. contributed in immunohistology staining and preparation of figures. I.D. and J.D. contributed in sample collection of patients with NMOSD and analysis of data and manuscript preparation. J.L.B. contributed human monoclonal antibodies, performed experiments for validation of antibodies, and contributed in the preparation of the manuscript. B.T.V. supervised and designed experimental procedures involving histology, analyzed data, and prepared the manuscript. P.T.H. supervised and analyzed experimental procedures for mouse behavior and neuronal recordings, prepared figures, and prepared the manuscript. B.D. conceived, designed, and supervised experimental procedures and prepared the manuscript.

Competing interests: The authors declare that they have no competing interests.

Abstract

The fetal brain is constantly exposed to maternal IgG before the formation of an effective blood-brain barrier (BBB). Here, we studied the consequences of fetal brain exposure to an antibody to the astrocytic protein aquaporin-4 (AQP4-IgG) in mice. AQP4-IgG was cloned from a patient with neuromyelitis optica spectrum disorder (NMOSD), an autoimmune disease that can affect women of childbearing age. We found that embryonic radial glia cells in neocortex express AQP4. These cells are critical for blood vessel and BBB formation through modulation of the WNT signaling pathway. Male fetuses exposed to AQP4-IgG had abnormal cortical vasculature and lower expression of WNT signaling molecules *Wnt5a* and *Wnt7a*. Positron emission tomography of adult male mice exposed in utero to AQP4-IgG revealed increased blood flow and BBB leakiness in the entorhinal cortex. Adult male mice exposed in utero to AQP4-IgG had abnormal cortical vessels, fewer dendritic spines in pyramidal and stellate neurons, and more $S100\beta^+$ astrocytes in the entorhinal cortex. Behaviorally, they showed impairments in the object-place memory task. Neural recordings indicated that their grid cell system, within the medial entorhinal cortex, did not map the local environment appropriately. Collectively, these data implicate in utero binding of AQP4-IgG to radial glia cells as a mechanism for alterations of the developing male brain and adds NMOSD to the conditions in which maternal IgG may cause persistent brain dysfunction in offspring.

INTRODUCTION

A family history of autoimmune diseases is associated with an increased risk of neurodevelopmental and neuropsychiatric disorders in the offspring. An increased risk for brain defects has been described in children born to mothers, but not fathers, with celiac disease, rheumatoid arthritis, and systemic lupus erythematosus (SLE) (1, 2). Neuromyelitis optica spectrum disorder (NMOSD) is an autoimmune disease causing demyelination of the optic nerves, brainstem, and spinal cord (3) affecting women of childbearing age (4). NMOSD is characterized by the presence of antibodies against the astrocytic protein aquaporin-4 (AQP4)–immunoglobulin G (IgG); these are present in nearly 80% of patients (5, 6) and contribute to disease pathogenesis. Administration of monoclonal AQP4-IgGs cloned from a patient with NMOSD into rodent models of experimental autoimmune encephalitis (7–9), or direct injection of AQP4-IgG into rodent brain (10), results in a phenotype that closely resembles NMOSD. Complement-dependent cytotoxicity (CDC) appears to be a major mechanism of tissue damage by AQP4-IgG (8, 10–12), but pathogenic T cells have also been implicated in brain injury (13, 14). Most studies in pregnant women with NMOSD focus on the effect of pregnancy on disease activity (15–18), although there are some reports of increased miscarriage and preeclampsia (4, 19), sometimes accompanied by multiple infarcts in the placenta (19). The available follow-up evidence for an effect of AQP4-IgG on neonates is sparse but includes cases of infants with hydrocephalus and persistent neurological impairment (4, 20). There are no long-term follow-up studies of children born to AQP4-IgG–positive mothers.

It is well established that in utero exposure to maternal autoantibodies present in other conditions can alter neurodevelopment as IgG can access the developing before the blood brain barrier (BBB) matures (21–23). For example, maternal antibodies that cross-react

with the *N*-methyl-D-aspartate receptor found in SLE lead to cognitive impairment in male offspring (24) and nonviability of female fetuses (25). Moreover, in a mouse model of autism spectrum disorders (ASDs), maternal antibodies against Contactin-a ssociated protein-like 2 (Caspr2) are associated with deficits in social interaction and repetitive behaviors in the offspring (26).

During embryonic development, AQP4 is expressed in radial glial cells (RGCs) of the developing cortex; however, by postpartum days 1 to 3, its expression is restricted to astrocytes (27). RGCs initially guide neuronal development, are the precursor cells for astrocytes (28–30), contribute to central nervous system (CNS) vascularization (31–34), and modulate wingless-type MMTV integration site family (WNT) signaling pathways in endothelial cells to stabilize newly formed blood vessels in the late embryonic brain (35). Although gene expression studies show that RGCs express *Aqp4* (36), its function in these cells is not completely elucidated. In the adult brain, AQP4 functions as a water channel that is localized in a polarized form at the endfeet of astrocytes that surround blood vessels.

Given the central role of RGCs in neurovascular development and the dearth of information about the cognitive outcome of children exposed in utero to maternal AQP4-IgG, we studied whether in utero exposure to an NMOSD patient-derived monoclonal AQP4-IgG would alter CNS vasculature development or lead to persistent functional and neurocognitive deficits.

RESULTS

AQP4 is expressed on radial glia in the fetal brain

We used quantitative polymerase chain reaction (qPCR) to quantify *Aqp4* gene expression in the fetal brain of mice and found that it increased steadily from embryonic day 11.5 (E11.5) to E18.5, whereas placental *Aqp4* expression was low throughout gestation (Fig. 1A). No differences in expression of *Aqp4* transcripts were observed between male and female fetal brains (Fig. 1A). The expression of embryonic AQP4 protein was demonstrated also by Western blot (Fig. 1B). Before E18.5, the dominant AQP4 band had a lower molecular weight than the adult form (Fig. 1B), which we reasoned might reflect the absence of glycosylation. AQP4 has two N-glycosylation sites. When we subjected adult AQP4 to enzymatic deglycosylation, it exhibited the same molecular weight as embryonic AQP4, suggesting that before E18.5, AQP4 was predominantly expressed as a nonglycosylated protein (fig. S1A).

We next confirmed a gene expression study showing that *Aqp4* is expressed in RGCs (36), by immunostaining of the fetal cortex at E14.5 with an antibody against the glutamate/aspartate transporter (GLAST), a marker for RGCs, and a commercially available anti-AQP4 antibody that recognizes embryonic AQP4 (Fig. 1C). At E14.5, AQP4 was expressed on both the soma and processes of $GLAST^+$ RGCs in the developing cortex (Fig. 1C).

Maternal AQP4-IgG causes vasculature impairment in the fetal brain

We verified that the monoclonal AQP4-IgG cloned from a patient with NMOSD (8), which gets transferred during pregnancy into the embryonic brain (37), was able to bind to fetal mouse brain (fig. S1B) and to human embryonic kidney (HEK)–293T cells expressing

either AQP4 containing both glycosylation sites and AQP4 with mutations in both sites that prevent glycosylation (fig. S1C). An isotype-matched antibody, 2B4-IgG, which is specific for measles virus (38) without any brain reactivity (fig. S1B), was used as a control (37). For our murine model of maternal IgG transfer, AQP4-IgG or 2B4-IgG was administered, by retro-orbital injection, to dams at E14.5 to generate offspring exposed in utero to AQP4-IgG (termed AQP4 mice henceforth) or 2B4-IgG (termed 2B4 mice). We chose E14.5 since, at this embryonic age, there is increased expression of AQP4 (Fig. 1A), and maternal antibodies can cross the placenta and access the brain before the embryonic BBB restricts antibody access (21, 37).

Because RGCs express AQP4 and are involved in blood vessel ingression in the developing cortex and stabilization of newly formed blood vessels in the late embryonic brain (35, 39), we analyzed the cortical vasculature of AQP4 and 2B4 fetal brains. Isolectin B4 (IB4) was used to stain vascular endothelial cells at E18.5, a time point when the vast majority of cortical vessels have reached their mature form (35). Comparisons of vessel length revealed that AQP4 males had longer blood vessels, which extended radially within the developing cortex, when compared to 2B4 males (Fig. 2A). In female offspring, there were no differences in vasculature in the developing cortex between AQP4 and 2B4 mice (fig. S2A).

In parallel, we found decreased expression of the WNT signaling molecules, *Wnt*5A and *Wnt7*A, in the cortex of AQP4 males compared to 2B4 males at postnatal day 0 (P0) (Fig. 2B). We found that *Wnt*5A expression was decreased around cortical endothelial cells of AQP4 males (Fig. 2C), suggesting that RGCs that are affected by AQP4-IgG may alter the cortical vasculature of AQP4 males (35).

The pathology of NMOSD involves AQP4-IgG–mediated CDC (10–12, 40). Eculizumab, a U.S. Food and Drug Administration– approved complement inhibitor, is effective in patients with NMOSD (12, 41). It was previously suggested that transfer of AQP4-IgG to pregnant dams together with coinjection of the human complement factor C1q would damage the placenta (42). We did not detect any overt placental defects in dams given AQP4-IgG. There was no placental neutrophilic inflammation, and there was comparable microscopic necrosis in the placentas of AQP4-IgG– and 2B4-IgG–exposed dams 48 hours after antibody administration (fig. S2B).

Maternal AQP4-IgG acts through CDC

CDC is the main process by which AQP4-IgG mediates tissue destruction in NMOSD (8, 11, 43–45). We asked whether the altered cortical vasculature in the AQP4-IgG–exposed fetal brain was mediated by CDC. To address this question, we first demonstrated that C1q was present in the fetal cortex. We quantified *C1q* gene expression by qPCR in C57BL/6 nonmanipulated fetuses and found that *C1q* was increasingly expressed in the cortex, starting at E11.5 to E18.5, until it reached adult expression (Fig. 2D). The placenta showed low *C1q* expression throughout gestation (Fig. 2D).

Next, we showed that AQP4-IgG could activate the mouse complement cascade, leading to membrane-attack-complex (MAC) formation. Specifically, HEK-293T cells transfected

with either wild-type AQP4 or AQP4 with mutations in both glycosylation sites, fused with green fluorescent protein, were incubated with AQP4-IgG and serum obtained from a male mouse (containing active complement). MAC formation was observed in HEK-293T cells expressing either wild-type or mutant AQP4 (Fig. 2E). Conversely, no to negligible MAC formation was detected on cells incubated with 2B4-IgG and mouse serum (Fig. 2E). MAC depositions were also evident in the cortex of AQP4 males at E16.5 (48 hours after dams were given AQP4-IgG or 2B4-IgG) by staining with antibody targeting the complement component C5b-9 (fig. S2C).

To strengthen the causal link between AQP4-IgG and C1q activation, we evaluated the effect of AQP4-IgG administration to pregnant *C1q* knockout (*C1q*$^{-/-}$) dams. Analysis of cortical blood vessels in E18.5 brains, with isolectin-IB4 staining, revealed no vascular abnormalities in AQP4-*C1q*$^{-/-}$ male mice compared to 2B4-*C1q*$^{-/-}$ male mice (Fig. 2F).

Adult AQP4 males have an impaired BBB in the entorhinal cortex

Because of the dense expression of AQP4 at the BBB and on the basis of our findings of vascular changes in the fetal brain, we assessed BBB integrity in the adult brain by conducting a positron emission tomography (PET) study with three different tracers: [^{18}F]-fluorodeoxyglucose (FDG) to assess metabolism, [^{11}C]-isoaminobutyric acid (AIB) to assess BBB permeability, and [^{15}O]-labeled water (H_2O) to measure blood flow. We found enhanced [^{11}C]-AIB and [^{15}O]-H_2O signals in the entorhinal cortex of AQP4 males compared to 2B4 males (Fig. 3, A and B, and Table 1), indicating increased blood flow and a compromised BBB. We found no change in [^{18}F]-FDG in the entorhinal cortex of the same mice, suggesting no differences in metabolism between groups (Table 1). Moreover, there were no differences between AQP4 and 2B4 females for [^{11}C]-AIB, [^{15}O]-H_2O, or [^{18}F]-FDG (Fig. 3B and Table 1). In addition, analysis of [^{11}C]-AIB signals in the entorhinal cortex of *C1q*$^{-/-}$ males revealed no differences between AQP4-*C1q*$^{-/-}$ mice and 2B4-*C1q*$^{-/-}$ controls (Fig. 3B and Table 1). Using an independent region-of-interest approach, based on standard anatomical atlases (46, 47), we confirmed increased blood flow and BBB permeability in AQP4 males in the entorhinal cortex, but not in other brain regions (table S1).

To understand whether the compromised BBB was associated with an altered volume of the compartments that contain cerebrospinal fluid (CSF) in the brain, we used images from [^{18}F]-FDG PET analyzed with a CSF template as previously published (48). AQP4 male but not APQ4 female mice had an increased CSF volume (Table 2). Moreover, expression of claudin-5, an essential tight-junction protein in endothelial cells, was reduced in AQP4 males compared to 2B4 controls (Fig. 3C). There was significantly more IgG in the CSF of AQP4 males compared to 2B4 controls ($P = 0.02$; Fig. 3D), further supporting that the BBB is compromised in AQP4 males.

Adult AQP4 males show impaired object-place memory

Behavioral assessments showed that AQP4 males exhibited no abnormalities compared to the 2B4 males in an observational screen, which revealed no differences in body weight, coat, grip strength, body tone, and several reflexes (table S2). Moreover, AQP4 males had no

deficit in an olfaction test (fig. S3A), the open-field test (fig. S3, B and C), the novel object recognition task (fig. S3D), and the Morris water-maze task (fig. S3E). AQP4 females were also not different from 2B4 females in these assays (table S2 and fig. S3).

In addition, we assessed AQP4 mice in the object-place memory (OPM) task, a spatial cognition test in which an animal recognizes that an object has been relocated to a novel location (Fig. 4A) (49). AQP4 male, but not AQP4 female, animals failed to discriminate between the moved object and the stable object (remaining in the same location), as tested by their OPM ratios (Fig 4, B and C). Conversely, 2B4 males and 2B4 females exhibited the expected bias toward the moved object in the test phase (Fig 4, B and C). To confirm that brain injury occurred through a complement-dependent pathway, we subjected $C1q^{-/-}$ mice to the OPM task and found normal OPM ratios for both male and female AQP4-$C1q^{-/-}$ and 2B4-$C1q^{-/-}$ mice (Fig. 4C).

Adult AQP4 males show disorganized grid cells in the medial entorhinal cortex

Because the OPM data indicated impaired spatial cognition in AQP4 males, and the PET results demonstrated that the entorhinal cortex was a particularly sensitive brain region, we sought to investigate its network function in vivo. Mice were preselected for these recordings based on their performance in the OPM task so that AQP4 males with the lowest OPM ratios and 2B4 males with positive OPM ratios were chosen. Mice were implanted with four-tetrode arrays targeted to the medial entorhinal cortex (fig. S4 for electrode location). After implantation surgery, the tetrodes were slowly lowered until clear single units were observed at a final depth of ~1 mm (superficial layers of the medial entorhinal cortex). Single-unit recordings were obtained in both groups, and individual units were isolated and classified as grid cells (50, 51) for further analysis (Fig. 4D). Firing-rate maps in 2B4 mice formed evenly spaced hexagonal grids across the environment, and the spatial autocorrelation for these maps showed a center with hexagonally arranged correlation peaks surrounding it. In the AQP4 group, the firing maps did not show evenly spaced hexagonal grids, and when the spatial autocorrelation was determined, peaks were distorted and did not form well-defined hexagons (Fig. 4E). Grid cells recorded in the AQP4 males had significantly lower firing rates ($P = 0.028$) and grid scores ($P = 0.027$) compared to the 2B4 males (Fig. 4F).

Adult AQP4 males have structural abnormalities in the entorhinal cortex

Blood vessels in the entorhinal cortex of adult male mice were stained with lectin. There was longer length and diameter in the AQP4 males compared to the 2B4 group (Fig. 5, A and B). Moreover, adult AQP4 males exhibited altered entorhinal AQP4 expression; specifically, they had increased AQP4 expression around blood vessels (fig. S5A).

Quantification of Golgi-stained entorhinal stellate neurons (Fig. 5C) and pyramidal cells (Fig. 5D) revealed that the dendritic length for each neuronal type was not different between AQP4 and 2B4 males (Fig. 5E). However, we observed a reduced number of dendritic spines on pyramidal and stellate cells in the AQP4 males when compared to 2B4 males (Fig. 5F). These differences appear to be specific to the entorhinal cortex, as pyramidal neurons of the CA1 region of the hippocampus were similar in their dendritic length and number of

spines between the AQP4 and 2B4 males (fig. S6). We also found an increased number of S100β-labeled astrocytes, counted in stereologically similar entorhinal regions in AQP4 males compared to 2B4 males (Fig. 5G).

AQP4 staining was not altered in the kidney of adult AQP4 males (fig. S5B) where AQP4 is abundantly expressed (52). The amount of albumin in the urine was not different between adult AQP4 and 2B4 mice (fig. S5C), further emphasizing that maternal AQP4-IgG exposure did not affect kidney development.

Human NMOSD serum antibodies bind both embryonic and adult AQP4

Because we found that, before E18.5, AQP4 was predominantly expressed as a nonglycosylated protein, we wanted to investigate whether patients' autoantibodies differentially bind to glycosylated ("adult") or nonglycosylated ("embryonic") AQP4. Patients with antibody to nonglycosylated AQP4 may be more at-risk having offspring affected by antibody exposure. We analyzed serum samples from 38 female patients with NMOSD for binding to wild-type AQP4 and AQP4 containing mutations in both glycosylation sites, using a cell-based assay (Table 3). Most sera (69%) exhibited binding to both forms of AQP4; however, 31% preferentially bound to wild-type AQP4 and less to AQP4 with mutations in both glycosylation sites, suggesting that the antibodies present in these patients might be less damaging to fetal brains.

DISCUSSION

Our study provides evidence that exposure to AQP4-IgG during pregnancy promotes neurodevelopmental impairment that persists throughout adulthood in the male mouse brain. Structural alteration of brain vasculature was associated with BBB impairment, disrupted neuronal function, and impaired cognitive performance. Our data strongly suggest that the effect of maternal AQP4-IgG is mediated through targeting of AQP4-IgG to RGCs that shape several processes in the developing cortex, including the architecture of the cortical vessels.

The adult brain typically requires an insult to the BBB in order for antibodies to penetrate brain tissue (22); alternatively, the entry of AQP4-IgG to the brain can occur at the BBB-deficient sites such as the area postrema (53), whereas the fetal brain with its developing, therefore incomplete, BBB is exposed to circulating maternal antibodies from E12.5 until around E16.5 (21). In a prior study, we showed that maternal AQP4-IgG penetrates rodent fetal brain tissue (37). Since the discovery of AQP4-IgG, in 2005 (6), few reports have described the effect of in utero exposure to AQP4-IgG on the developing fetus. In mice, intraperitoneal injection of high titers of AQP4-IgG together with human complement resulted in fetal death and placental inflammation, whereas administration of lower amount of AQP4-IgG and human complement resulted in normal litter size, but no other observations of the offspring were performed (42). We did not observe any inflammation of the placenta. It is possible that higher concentrations of AQP4-IgG could affect the placenta or that high amount of human complement contributed to the placental damage. Our pregnancy model does not entirely recapitulate the features of the human disease; we cannot exclude that inflammation present in patients with NMOSD may have additional

deleterious effects on pregnancy. Clinical studies have reported a higher rate of miscarriages in AQP4-IgG–seropositive patients with NMOSD, which might reflect either placental or fetal injury (4). There are also two case reports of children with hydrocephalus born to AQP4-IgG–seropositive patients with NMOSD (4, 20), yet mostly normal births have been reported (4, 20). However, to our knowledge, there are no long-term epidemiological studies assessing cognitive function and neurodevelopmental outcomes in boys and girls born to AQP4-IgG–positive mothers with NMOSD.

We have found that AQP4 is expressed in the brain at a time when maternal antibodies can penetrate the embryonic brain in mice. In the adult brain, AQP4 is expressed on astrocytic endfeet. Since astrocytes appear rather late in development, we asked which cells express AQP4 in the fetal brain. A previous study reported AQP4 expression on RGCs in the developing cortex (27). In addition, whole transcriptome data during mouse brain development showed that *Aqp4* is expressed in proliferating progenitor cells, much less in differentiating progenitor cells, and not in postmitotic neurons (36). This pattern of *Aqp4* expression is similar to the expression of *Sox2* (36), a marker for RGCs. We have found that the AQP4 protein is expressed in $GLAST^+$ RGCs as early as E14.5. Furthermore, we established that AQP4 expressed in the fetal brain has a lower molecular weight than the adult brain, likely due to lack of glycosylation.

In our model, male but not female mice exposed in utero to AQP4-IgG showed altered brain vasculature associated with changes in expression of WNT signaling molecules. A critical clue to this sex-specific phenotype comes from the observation that $C1q^{-/-}$ male mice exposed in utero to AQP4-IgG did not have alterations in brain vasculature. This result clearly implicates the complement cascade in the effect of AQP4-IgG. Complement genes are expressed in a sexually dimorphic pattern, so that during neocortical development, complement genes are more highly expressed in males than females (54). In adulthood, the pattern reverses, and complement genes are more expressed in females (54). Thus, a differential expression of complement components may explain why males, but not females, are affected when they are exposed in utero to AQP4-IgG. Of note, maternal antibodies have also been shown to affect neurodevelopment in a sex-dependent manner in SLE and ASD (24, 26).

Our study suggests that maternal AQP4-IgG–mediated fetal brain injury is complement dependent. Although mouse complement can be activated in vivo by antibodies with a human Fc region (55, 56), we are also aware of data showing that human AQP4-IgG needs to be coinjected with human complement to cause pathology in mouse models of NMOSD (10, 57, 58). The discrepancy between our data and previous reports may reflect differences in the abundance and/or function of complement components between the fetal and adult complement systems.

It is likely that AQP4-IgG interferes with the normal interaction of RGCs and endothelial cells leading to abnormal vasculature in the cortex at a critical developmental time. Ablation of RGCs interferes with the sprouting of the trunk vessels in the spinal cord of zebrafish embryos (59) and alters the vasculature in the fetal cortex of rodents (35). Deletion of AQP4 in mice has been linked to impaired synaptic plasticity and poor performance in the

OPM task (60, 61). We found that in utero exposure to maternal AQP4-IgG produced a vasculature phenotype in the male brain, by E18.5, which continued into adulthood. Our data point to the entorhinal cortex as a focal node in the adult brain for the persistence of the neurodevelopmental impairment. More studies are needed to understand the specific fragility of the entorhinal cortex to AQP4-IgG, but our work demonstrates that both structural and functional abnormalities associate with impaired spatial cognition.

Deficient vasculature development can lead to neurodevelopmental defects. For instance, glucose transporter 1 (GLUT1) deficiency syndrome, a genetic disease characterized by a lack of GLUT1 in the brain, leads to delayed brain angiogenesis and reduced size of microvasculature without affecting BBB integrity (62). Early repletion of GLUT1 restores cerebral microvasculature (62). Several studies have associated BBB dysfunction with cognitive impairment (63–65). For example, mice lacking apolipoprotein E (ApoE), a model for late Alzheimer's disease, show BBB leakage accompanied by cognitive deficits including memory impairment (66–68). Aging ApoE-deficient mice exhibit altered AQP4 expression, which possibly contributes to the BBB impairment. BBB leakage can result in disturbance of ionic homeostasis and thus can lead to neuronal dysregulation. Vascular pathology can lead to increased S100β expression (69). Furthermore, stress can also lead to increased S100β expression (70). It is intriguing that investigators have demonstrated elevated S100β concentration in the CSF of patients with NMOSD, which may reflect astrocytic damage due to pathogenic AQP4-IgG (71–73).

We demonstrated that a vasculature phenotype may be caused by maternal AQP4-IgG affecting RGCs and blood vessel structure via WNT signaling. The combination of neuronal alterations and leaky BBB in the entorhinal cortex suggests that a dysfunctional BBB may be driving the neuronal phenotype (74, 75). We cannot exclude the idea that early exposure to AQP4-IgG affects neuronal/astrocyte precursors leading to long-term neuronal dysfunction. Note that BBB impairment was specific to the entorhinal cortex. The entorhinal cortex is one of the first cortical regions to initiate neurogenesis (76), and AQP4 is highly expressed in adult entorhinal cortex (77), possibly making it more vulnerable to the effect of circulating AQP4-IgG during a critical time of development.

The main limitation of our study is that murine models might have different effector functions, and thus humanized models or studies in nonhuman primates are warranted to further elucidate the role of maternal AQP4 antibodies. In addition, there is only limited information regarding the effect of in utero exposure to AQP4-IgG in humans with no longitudinal follow-up studies. Future studies are needed to assess larger cohorts of children born to mothers with AQP4-IgG, which also need to address the effects of maternal medication or indirect effects of maternal illness, such as cytokines or pathogenic T cells. It is also possible that additional factors such as genetics and in utero environmental variables contribute to the effect of maternal AQP4-IgG on development.

Our study is particularly important, as earlier diagnosis and appropriate treatment greatly improve clinical outcome of patients and may increase the number of successful pregnancies of patients with NMOSD. Demonstrating how maternal brain-reactive autoantibodies can interfere with the developing brain and lead to a durable effect represents an important

step toward the initiation of long-term studies in humans and the development of future therapeutic interventions. It also increases our understanding of the development of the brain microvasculature.

MATERIALS AND METHODS

Study design

Our goal was to investigate the acute and long-term effect of in utero exposure to maternal AQP4-IgG on the developing brain. AQP4 expression was assessed in the developing brain. The brains of embryos and adult AQP4 mice, as well as 2B4 mice, were analyzed histologically for alterations in endothelial cells, astrocytes, and neurons. Adult mice were evaluated with a microPET study to measure BBB integrity and IgG infiltration into the CSF. Adult mice were also assessed with behavioral tests, including the OPM task for spatial cognition, and an electrophysiological study of the entorhinal cortex. No statistical methods were used to predetermine sample size. No data were excluded from analyses. The animals were randomly assigned to the behavioral testing, microPET, and histological analysis except for the preselection of animals for neuronal recordings, as stated in the appropriate section. All animals were run in random order by investigators blinded to the treatment group of each animal. Information regarding number of samples and experimental replicates is indicated per experiment in each figure legend.

Animals

We used adult C57BL/6 mice (the Jackson Laboratory, strain #000664) as well as *C1q*$^{-/-}$ mice on a C57BL/6 background, which were bred to C57BL/6-H2d haplotype. Mice were, on average, 3 to 5 months old unless otherwise specified. *C1q*$^{-/-}$ mice were obtained from V. S. Ten (Department of Pediatrics, Columbia University). All mice were housed with ad libitum access to food and water. The animals' care was in accordance with the National Institutes of Health Guidelines under protocols reviewed and approved by the Institutional Animal Care and Use Committee (2009–048 and 2013–014) of the Feinstein Institutes for Medical Research.

Human monoclonal antibodies

AQP4-IgG rAb-53 was cloned from a patient with NMOSD, and specificity of the antibody for AQP4 binding was previously confirmed (8). The isotype-control recombinant 2B4-IgG binds to measles virus nucleocapsid protein (38). Antibody concentrations were measured by IgG enzyme-linked immunosorbent assay (37) and Nanodrop. Each new batch of recombinant human AQP4-IgG (1 μg/ml) is verified to bind to human AQP4 using a cell-based assay with HEK-293T cells (American Type Culture Collection, CRL 11268TM) transiently transfected with AQP4 (78). Monoclonal antibody was tested for binding to cells expressing AQP4 (M23 isoform) as well as cells expressing nonglycosylated AQP4 as described below. Nontransfected cells and cells expressing a nonrelevant protein (Caspr2) were included as negative controls.

Serum binding to glycosylated and nonglycosylated forms of AQP4

Serum of patients was collected at the Clinic of Neurology, Clinical Center of Serbia. All patients met the revised diagnostic criteria of NMOSD (3). Individuals provided informed consent through the appropriate institutional review boards. Participation in this research was approved by the University of Belgrade Faculty of Medicine Institutional Review Board (approval number 29/X-8, amendment approval number 1322/XII-22). Serum of 38 patients with NMSOD was tested for IgG binding to human AQP4 (plasmid provided as a gift from M. Reindl) and nonglycosylated human AQP4 (see the Supplementary Materials) expressed on the cell surface of HEK-293T cells as previously described (78, 79). Antibody titers were analyzed by serial dilution until no more signal of AQP4-IgG binding was observed.

Statistical analysis

All raw, individual-level data are presented in data file S1. We performed the Shapiro-Wilk normality test in each dataset to determine whether the sample was drawn from a normally distributed population. We then used Student's t test for datasets that were normally distributed (and with samples larger than 10). For small datasets that were not normally distributed (sample sizes less than 10), we performed the Mann-Whitney U test. For large datasets that were not normally distributed, we used the Kolmogorov-Smirnov test. For dendritic branching datasets from neurons, we used a linear mixed model. To analyze categorical data, we used a χ^2-test for independence. All tests were performed with the statistical tool-box of OriginPro (version 2021b, 64 bit, SR2, OriginLab Corp.) and are indicated in the text. Values were considered significant for $P < 0.05$. Data are presented as mean, and error bars represent standard error. All tests were performed two-tailed.

Supplementary Material

Refer to Web version on PubMed Central for supplementary material.

Acknowledgments:

We thank C. Kowal for assistance in perfusing embryos, J. Nestor for assistance in obtaining CSF through cisterna-magna-puncture, C. Bagnall-Moreau for assistance with MBF ImageJ software, and C. Haupt for helpful discussions.

Funding:

This work was supported by NIH Grants 5P01AI102852 (to B.D.), 5P01AI073693 (to B.D.), and 2R01EY022936 (to J.L.B.); by the DOD impact award W81XWH1910759 (to P.T.H.); and by the Guthy Jackson Charitable Foundation (to J.L.B.).

Data and materials availability:

All data associated with this study are present in the paper or the Supplementary Materials.

REFERENCES AND NOTES

1. Atladottir HO, Pedersen MG, Thorsen P, Mortensen PB, Deleuran B, Eaton WW, Parner ET, Association of family history of autoimmune diseases and autism spectrum disorders. Pediatrics 124, 687–694 (2009). [PubMed: 19581261]

2. Vinet E, Pineau CA, Clarke AE, Scott S, Fombonne E, Joseph L, Platt RW, Bernatsky S, Increased risk of autism spectrum disorders in children born to women with systemic lupus erythematosus: Results from a large population-based cohort. Arthritis Rheumatol. 67, 3201–3208 (2015). [PubMed: 26315754]

3. Wingerchuk DM, Banwell B, Bennett JL, Cabre P, Carroll W, Chitnis T, de Seze J, Fujihara K, Greenberg B, Jacob A, Jarius S, Lana-Peixoto M, Levy M, Simon JH, Tenembaum S, Traboulsee AL, Waters P, Wellik KE, Weinshenker BG; International Panel for NMO Diagnosis, International consensus diagnostic criteria for neuromyelitis optica spectrum disorders. Neurology 85, 177–189 (2015). [PubMed: 26092914]

4. Nour MM, Nakashima I, Coutinho E, Woodhall M, Sousa F, Revis J, Takai Y, George J, Kitley J, Santos ME, Nour JM, Cheng F, Kuroda H, Misu T, Martins-da-Silva A, DeLuca GC, Vincent A, Palace J, Waters P, Fujihara K, Leite MI, Pregnancy outcomes in aquaporin-4-positive neuromyelitis optica spectrum disorder. Neurology 86, 79–87 (2016). [PubMed: 26581304]

5. Waters P, Jarius S, Littleton E, Leite MI, Jacob S, Gray B, Geraldes R, Vale T, Jacob A, Palace J, Maxwell S, Beeson D, Vincent A, Aquaporin-4 antibodies in neuromyelitis optica and longitudinally extensive transverse myelitis. Arch. Neurol 65, 913–919 (2008). [PubMed: 18625857]

6. Lennon VA, Kryzer TJ, Pittock SJ, Verkman AS, Hinson SR, IgG marker of optic-spinal multiple sclerosis binds to the aquaporin-4 water channel. J. Exp. Med 202, 473–477 (2005). [PubMed: 16087714]

7. Bradl M, Misu T, Takahashi T, Watanabe M, Mader S, Reindl M, Adzemovic M, Bauer J, Berger T, Fujihara K, Itoyama Y, Lassmann H, Neuromyelitis optica: Pathogenicity of patient immunoglobulin in vivo. Ann. Neurol 66, 630–643 (2009). [PubMed: 19937948]

8. Bennett JL, Lam C, Kalluri SR, Saikali P, Bautista K, Dupree C, Glogowska M, Case D, Antel JP, Owens GP, Gilden D, Nessler S, Stadelmann C, Hemmer B, Intrathecal pathogenic anti-aquaporin-4 antibodies in early neuromyelitis optica. Ann. Neurol 66, 617–629 (2009). [PubMed: 19938104]

9. Hillebrand S, Schanda K, Nigritinou M, Tsymala I, Bohm D, Peschl P, Takai Y, Fujihara K, Nakashima I, Misu T, Reindl M, Lassmann H, Bradl M, Circulating AQP4-specific auto-antibodies alone can induce neuromyelitis optica spectrum disorder in the rat. Acta Neuropathol. 137, 467–485 (2019). [PubMed: 30564980]

10. Saadoun S, Waters P, Bell BA, Vincent A, Verkman AS, Papadopoulos MC, Intra-cerebral injection of neuromyelitis optica immunoglobulin G and human complement produces neuromyelitis optica lesions in mice. Brain 133, 349–361 (2010). [PubMed: 20047900]

11. Soltys J, Liu Y, Ritchie A, Wemlinger S, Schaller K, Schumann H, Owens GP, Bennett JL, Membrane assembly of aquaporin-4 autoantibodies regulates classical complement activation in neuromyelitis optica. J. Clin. Invest 129, 2000–2013 (2019). [PubMed: 30958797]

12. Pittock SJ, Berthele A, Fujihara K, Kim HJ, Levy M, Palace J, Nakashima I, Terzi M, Totolyan N, Viswanathan S, Wang KC, Pace A, Fujita KP, Armstrong R, Wingerchuk DM, Eculizumab in aquaporin-4-positive neuromyelitis optica spectrum disorder. N. Engl. J. Med 381, 614–625 (2019). [PubMed: 31050279]

13. Zeka B, Hastermann M, Hochmeister S, Kogl N, Kaufmann N, Schanda K, Mader S, Misu T, Rommer P, Fujihara K, Illes Z, Leutmezer F, Sato DK, Nakashima I, Reindl M, Lassmann H, Bradl M, Highly encephalitogenic aquaporin 4-specific T cells and NMO-IgG jointly orchestrate lesion location and tissue damage in the CNS. Acta Neuropathol. 130, 783–798 (2015). [PubMed: 26530185]

14. Pohl M, Kawakami N, Kitic M, Bauer J, Martins R, Fischer MT, Machado-Santos J, Mader S, Ellwart JW, Misu T, Fujihara K, Wekerle H, Reindl M, Lassmann H, Bradl M, T cell-activation in neuromyelitis optica lesions plays a role in their formation. Acta Neuropathol. Commun 1, 85 (2013). [PubMed: 24367907]

15. Kim W, Kim SH, Nakashima I, Takai Y, Fujihara K, Leite MI, Kitley J, Palace J, Santos E, Coutinho E, Silva AM, Kim BJ, Kim BJ, Ahn SW, Kim HJ, Influence of pregnancy on neuromyelitis optica spectrum disorder. Neurology 78, 1264–1267 (2012). [PubMed: 22491862]

16. Fragoso YD, Adoni T, Bichuetti DB, Brooks JB, Ferreira ML, Oliveira EM, Oliveira CL, Ribeiro SB, Silva AE, Siquineli F, Neuromyelitis optica and pregnancy. Neurol. 260, 2614–2619 (2013).

17. Bourre B, Marignier R, Zephir H, Papeix C, Brassat D, Castelnovo G, Collongues N, Vukusic S, Labauge P, Outteryck O, Fontaine B, Vermersch P, Confavreux C, de Seze J; NOMADMUS Study Group, Neuromyelitis optica and pregnancy. Neurology 78, 875–879 (2012). [PubMed: 22402855]
18. Shimizu Y, Fujihara K, Ohashi T, Nakashima I, Yokoyama K, Ikeguch R, Takahashi T, Misu T, Shimizu S, Aoki M, Kitagawa K, Pregnancy-related relapse risk factors in women with anti-AQP4 antibody positivity and neuromyelitis optica spectrum disorder. Mult. Scler 22, 1413–1420 (2016). [PubMed: 25921053]
19. Reuss R, Rommer PS, Bruck W, Paul F, Bolz M, Jarius S, Boettcher T, Grossmann A, Bock A, Zipp F, Benecke R, Zettl UK, A woman with acute myelopathy in pregnancy: Case outcome. BMJ 339, b4026 (2009).
20. Huang Y, Wang Y, Zhou Y, Huang Q, Sun X, Chen C, Fang L, Long Y, Yang H, Wang H, Li C, Lu Z, Hu X, Kermode AG, Qiu W, Pregnancy in neuromyelitis optica spectrum disorder: A multicenter study from South China. J. Neurol. Sci 372, 152–156 (2017). [PubMed: 28017203]
21. Braniste V, Al-Asmakh M, Kowal C, Anuar F, Abbaspour A, Toth M, Korecka A, Bakocevic N, Ng LG, Kundu P, Gulyas B, Halldin C, Hultenby K, Nilsson H, Hebert H, Volpe BT, Diamond B, Pettersson S, The gut microbiota influences blood-brain barrier permeability in mice. Sci. Transl. Med 6, 263ra158 (2014).
22. Diamond B, Honig G, Mader S, Brimberg L, Volpe BT, Brain-reactive antibodies and disease. Annu. Rev. Immunol 31, 345–385 (2013). [PubMed: 23516983]
23. Brimberg L, Mader S, Fujieda Y, Arinuma Y, Kowal C, Volpe BT, Diamond B, Antibodies as mediators of brain pathology. Trends Immunol. 36, 709–724 (2015). [PubMed: 26494046]
24. Lee JY, Huerta PT, Zhang J, Kowal C, Bertini E, Volpe BT, Diamond B, Neurotoxic autoantibodies mediate congenital cortical impairment of offspring in maternal lupus. Nat. Med 15, 91–96 (2009). [PubMed: 19079257]
25. Wang L, Zhou D, Lee J, Niu H, Faust TW, Frattini S, Kowal C, Huerta PT, Volpe BT, Diamond B, Female mouse fetal loss mediated by maternal autoantibody. J. Exp. Med 209, 1083–1089 (2012). [PubMed: 22565825]
26. Brimberg L, Mader S, Jeganathan V, Berlin R, Coleman TR, Gregersen PK, Huerta PT, Volpe BT, Diamond B, Caspr2-reactive antibody cloned from a mother of an ASD child mediates an ASD-like phenotype in mice. Mol. Psychiatry 21, 1663–1671 (2016). [PubMed: 27698429]
27. Fallier-Becker P, Vollmer JP, Bauer HC, Noell S, Wolburg H, Mack AF, Onset of aquaporin-4 expression in the developing mouse brain. Int. J. Dev. Neurosci 36, 81–89 (2014). [PubMed: 24915007]
28. Marin O, Rubenstein JL, Cell migration in the forebrain. Annu. Rev. Neurosci 26, 441–483 (2003). [PubMed: 12626695]
29. Rakic P, Elusive radial glial cells: Historical and evolutionary perspective. Glia 43, 19–32 (2003). [PubMed: 12761862]
30. Segarra M, Kirchmaier BC, Acker-Palmer A, A vascular perspective on neuronal migration. Mech. Dev 138 Pt 1, 17–25 (2015). [PubMed: 26192337]
31. Liebner S, Corada M, Bangsow T, Babbage J, Taddei A, Czupalla CJ, Reis M, Felici A, Wolburg H, Fruttiger M, Taketo MM, von Melchner H, Plate KH, Gerhardt H, Dejana E, Wnt/beta-catenin signaling controls development of the blood-brain barrier. Cell Biol. 183, 409–417 (2008).
32. Daneman R, Agalliu D, Zhou L, Kuhnert F, Kuo CJ, Barres BA, Wnt/beta-catenin signaling is required for CNS, but not non-CNS, angiogenesis. Proc. Natl. Acad. Sci. U.S.A 106, 641–646 (2009). [PubMed: 19129494]
33. Stenman JM, Rajagopal J, Carroll TJ, Ishibashi M, McMahon J, McMahon AP, Canonical Wnt signaling regulates organ-specific assembly and differentiation of CNS vasculature. Science 322, 1247–1250 (2008). [PubMed: 19023080]
34. Raab S, Beck H, Gaumann A, Yuce A, Gerber HP, Plate K, Hammes HP, Ferrara N, Breier G, Impaired brain angiogenesis and neuronal apoptosis induced by conditional homozygous inactivation of vascular endothelial growth factor. Thromb. Haemost 91, 595–605 (2004). [PubMed: 14983237]
35. Ma S, Kwon HJ, Johng H, Zang K, Huang Z, Radial glial neural progenitors regulate nascent brain vascular network stabilization via inhibition of Wnt signaling. PLoS Biol. 11, e1001469 (2013).

36. Aprea J, Prenninger S, Dori M, Ghosh T, Monasor LS, Wessendorf E, Zocher S, Massalini S, Alexopoulou D, Lesche M, Dahl A, Groszer M, Hiller M, Calegari F, Transcriptome sequencing during mouse brain development identifies long non-coding RNAs functionally involved in neurogenic commitment. EMBO J. 32, 3145–3160 (2013). [PubMed: 24240175]
37. Mader S, Brimberg L, Soltys JN, Bennett JL, Diamond B, Mutations of recombinant aquaporin-4 antibody in the Fc domain can impair complement-dependent cellular cytotoxicity and transplacental transport. Front. Immunol 9, 1599 (2018). [PubMed: 30057582]
38. Burgoon MP, Williamson RA, Owens GP, Ghausi O, Bastidas RB, Burton DR, Gilden DH, Cloning the antibody response in humans with inflammatory CNS disease: Isolation of measles virus-specific antibodies from phage display libraries of a subacute sclerosing panencephalitis brain. J. Neuroimmunol 94, 204–211 (1999). [PubMed: 10376954]
39. Matsuoka RL, Rossi A, Stone OA, Stainier DYR, CNS-resident progenitors direct the vascularization of neighboring tissues. Proc. Natl. Acad. Sci. U.S.A 114, 10137–10142 (2017). [PubMed: 28855341]
40. Hinson SR, Romero MF, Popescu BF, Lucchinetti CF, Fryer JP, Wolburg H, Fallier-Becker P, Noell, Lennon VA, Molecular outcomes of neuromyelitis optica (NMO)-IgG binding to aquaporin-4 in astrocytes. Proc. Natl. Acad. Sci. U.S.A 109, 1245–1250 (2012). [PubMed: 22128336]
41. Palace J, Wingerchuk DM, Fujihara K, Berthele A, Oreja-Guevara C, Kim HJ, Nakashima I, Levy M, Terzi M, Totolyan N, Viswanathan S, Wang KC, Pace A, Yountz M, Miller L, Armstrong R, Pittock S; PREVENT Study Group, Benefits of eculizumab in AQP4+ neuromyelitis optica spectrum disorder: Subgroup analyses of the randomized controlled phase 3 PREVENT trial. Mult. Scler. Relat. Disord 47, 102641 (2021). [PubMed: 33310418]
42. Saadoun S, Waters P, Leite MI, Bennett JL, Vincent A, Papadopoulos MC, Neuromyelitis optica IgG causes placental inflammation and fetal death. J. Immunol 191, 2999–3005 (2013). [PubMed: 23935196]
43. Hinson SR, McKeon A, Fryer JP, Apiwattanakul M, Lennon VA, Pittock SJ, Prediction of neuromyelitis optica attack severity by quantitation of complement-mediated injury to aquaporin-4-expressing cells. Arch. Neurol 66, 1164–1167 (2009). [PubMed: 19752309]
44. Roemer SF, Parisi JE, Lennon VA, Benarroch EE, Lassmann H, Bruck W, Mandler RN, Weinshenker BG, Pittock SJ, Wingerchuk DM, Lucchinetti CF, Pattern-specific loss of aquaporin-4 immunoreactivity distinguishes neuromyelitis optica from multiple sclerosis. Brain 130, 1194–1205 (2007). [PubMed: 17282996]
45. Sabater L, Giralt A, Boronat A, Hankiewicz K, Blanco Y, Llufriu S, Alberch J, Graus F, Saiz A, Cytotoxic effect of neuromyelitis optica antibody (NMO-IgG) to astrocytes: An in vitro study. J. Neuroimmunol 215, 31–35 (2009). [PubMed: 19695715]
46. Johnson GA, Badea A, Brandenburg J, Cofer G, Fubara B, Liu S, Nissanov J, Waxholm space: An image-based reference for coordinating mouse brain research. Neuroimage 53, 365–372 (2010). [PubMed: 20600960]
47. Ullmann JFP, Watson C, Janke AL, Kurniawan ND, Reutens DC, A segmentation protocol and MRI atlas of the C57BL/6J mouse neocortex. Neuroimage 78, 196–203 (2013). [PubMed: 23587687]
48. Sawiak SJ, Wood NI, Williams GB, Morton AJ, Carpenter TA, Voxel-based morphometry in the R6/2 transgenic mouse reveals differences between genotypes not seen with manual 2D morphometry. Neurobiol. Dis 33, 20–27 (2009). [PubMed: 18930824]
49. Faust TW, Robbiati S, Huerta TS, Huerta PT, Dynamic NMDAR-mediated properties of place cells during the object place memory task. Front. Behav. Neurosci 7, 202 (2013). [PubMed: 24381547]
50. Fyhn M, Hafting T, Witter MP, Moser EI, Moser MB, Grid cells in mice. Hippocampus 18, 1230–1238 (2008). [PubMed: 18683845]
51. Miao C, Cao Q, Moser MB, Moser EI, Parvalbumin and somatostatin interneurons control different space-coding networks in the medial entorhinal cortex. Cell 171, 507–521.e17 (2017). [PubMed: 28965758]
52. Nielsen S, Agre P, The aquaporin family of water channels in kidney. Kidney Int. 48, 1057–1068 (1995). [PubMed: 8569067]

53. Shosha E, Dubey D, Palace J, Nakashima I, Jacob A, Fujihara K, Takahashi T, Whittam D, Leite MI, Misu T, Yoshiki T, Messina S, Elsone L, Majed M, Flanagan E, Gadoth A, Huebert C, Sagen J, Greenberg BM, Levy M, Banerjee A, Weinshenker B, Pittock SJ, Area postrema syndrome: Frequency, criteria, and severity in AQP4-IgGpositive NMOSD. Neurology 91, e1642–e1651 (2018). [PubMed: 30258024]
54. Prilutsky D, Kho A, Feiglin A, Hammond T, Stevens B, Kohane IS, Sexual dimorphism of complement-dependent microglial synaptic pruning and other immune pathways in the developing brain. biorxiv 204412 [Preprint] (2017). 10.1101/204412.
55. Di Gaetano N, Cittera E, Nota R, Vecchi A, Grieco V, Scanziani E, Botto M, Introna M, Golay J, Complement activation determines the therapeutic activity of rituximab in vivo. Immunol. 171, 1581–1587 (2003).
56. Saeland E, Vidarsson G, Leusen JH, Van Garderen E, Nahm MH, Vile-Weekhout H, Walraven V, Stemerding AM, Verbeek JS, Rijkers GT, Kuis W, Sanders EA, Van De Winkel JG, Central role of complement in passive protection by human IgG1 and IgG2 anti-pneumococcal antibodies in mice. J. Immunol 170, 6158–6164 (2003). [PubMed: 12794146]
57. Zhang H, Verkman AS, Longitudinally extensive NMO spinal cord pathology produced by passive transfer of NMO-IgG in mice lacking complement inhibitor CD59. J. Autoimmun 53, 67–77 (2014). [PubMed: 24698947]
58. Asavapanumas N, Ratelade J, Papadopoulos MC, Bennett JL, Levin MH, Verkman AS, Experimental mouse model of optic neuritis with inflammatory demyelination produced by passive transfer of neuromyelitis optica-immunoglobulin G. J. Neuroinflammation 11, 16 (2014). [PubMed: 24468108]
59. Matsuoka RL, Marass M, Avdesh A, Helker CS, Maischein HM, Grosse AS, Kaur H, Lawson ND, Herzog W, Stainier DY, Radial glia regulate vascular patterning around the developing spinal cord. eLife 5, e20253 (2016).
60. Skucas VA, Mathews IB, Yang J, Cheng Q, Treister A, Duffy AM, Verkman AS, Hempstead BL, Wood MA, Binder DK, Scharfman HE, Impairment of select forms of spatial memory and neurotrophin-dependent synaptic plasticity by deletion of glial aquaporin-4. J. Neurosci 31, 6392–6397 (2011). [PubMed: 21525279]
61. Scharfman HE, Binder DK, Aquaporin-4 water channels and synaptic plasticity in the hippocampus. Neurochem. Int 63, 702–711 (2013). [PubMed: 23684954]
62. Tang M, Gao G, Rueda CB, Yu H, Thibodeaux DN, Awano T, Engelstad KM, Sanchez-Quintero MJ, Yang H, Li F, Li H, Su Q, Shetler KE, Jones L, Seo R, McConathy J, Hillman EM, Noebels JL, De Vivo DC, Monani UR, Brain microvasculature defects and Glut1 deficiency syndrome averted by early repletion of the glucose transporter-1 protein. Nat. Commun 8, 14152 (2017). [PubMed: 28106060]
63. Geng J, Wang L, Zhang L, Qin C, Song Y, Ma Y, Chen Y, Chen S, Wang Y, Zhang Z, Yang GY, Blood-brain barrier disruption induced cognitive impairment is associated with increase of inflammatory cytokine. Front. Aging Neurosci 10, 129 (2018). [PubMed: 29867440]
64. Mogi M, Horiuchi M, Neurovascular coupling in cognitive impairment associated with diabetes mellitus. Circ. J 75, 1042–1048 (2011). [PubMed: 21441696]
65. Taheri S, Gasparovic C, Huisa BN, Adair JC, Edmonds E, Prestopnik J, Grossetete M, Shah NJ, Wills J, Qualls C, Rosenberg GA, Blood-brain barrier permeability abnormalities in vascular cognitive impairment. Stroke 42, 2158–2163 (2011). [PubMed: 21719768]
66. Hafezi-Moghadam A, Thomas KL, Wagner DD, ApoE deficiency leads to a progressive age-dependent blood-brain barrier leakage. Am. J. Phys. Cell Physiol 292, C1256–C1262 (2007).
67. Fullerton SM, Shirman GA, Strittmatter WJ, Matthew WD, Impairment of the bloodnerve and blood-brain barriers in apolipoprotein E knockout mice. Exp. Neurol 169, 13–22 (2001). [PubMed: 11312553]
68. Methia N, Andre P, Hafezi-Moghadam A, Economopoulos M, Thomas KL, Wagner DD, ApoE deficiency compromises the blood brain barrier especially after injury. Mol. Med 7, 810–815 (2001). [PubMed: 11844869]

69. Kalinichenko SG, Korobtsov AV, Matveeva NY, Pushchin II, Structural and chemical changes in glial cells in the rat neocortex induced by constant occlusion of the middle cerebral artery. Acta Histochem. 122, 151573 (2020). [PubMed: 32622419]

70. Gerlai R, Wojtowicz JM, Marks A, Roder J, Overexpression of a calcium-binding protein, S100 beta, in astrocytes alters synaptic plasticity and impairs spatial learning in transgenic mice. Learn. Mem 2, 26–39 (1995). [PubMed: 10467564]

71. Takano R, Misu T, Takahashi T, Sato S, Fujihara K, Itoyama Y, Astrocytic damage is far more severe than demyelination in NMO: A clinical CSF biomarker study. Neurology 75, 208–216 (2010). [PubMed: 20644148]

72. Wei Y, Chang H, Li X, Du L, Xu W, Cong H, Yao Y, Zhang X, Yin L, CSF-S100B is a potential candidate biomarker for neuromyelitis optica spectrum disorders. Biomed. Res. Int 2018, 5381239 (2018). [PubMed: 30426010]

73. Misu T, Takano R, Fujihara K, Takahashi T, Sato S, Itoyama Y, Marked increase in cerebrospinal fluid glial fibrillar acidic protein in neuromyelitis optica: An astrocytic damage marker. J. Neurol. Neurosurg. Psychiatry 80, 575–577 (2009). [PubMed: 19372295]

74. Zlokovic BV, The blood-brain barrier in health and chronic neurodegenerative disorders. Neuron 57, 178–201 (2008). [PubMed: 18215617]

75. Ju F, Ran Y, Zhu L, Cheng X, Gao H, Xi X, Yang Z, Zhang S, Increased BBB permeability enhances activation of microglia and exacerbates loss of dendritic spines after transient global cerebral ischemia. Front. Cell. Neurosci 12, 236 (2018). [PubMed: 30123113]

76. Liu Y, Bergmann T, Mori Y, Peralvo Vidal JM, Pihl M, Vasistha NA, Thomsen PD, Seemann SE, Gorodkin J, Hyttel P, Khodosevich K, Witter MP, Hall VJ, Development of the entorhinal cortex occurs via parallel lamination during neurogenesis. Front. Neuroanat 15, 663667 (2021). [PubMed: 34025365]

77. Aoyama M, Kakita H, Kato S, Tomita M, Asai K, Region-specific expression of a water channel protein, aquaporin 4, on brain astrocytes. J. Neurosci. Res 90, 2272–2280 (2012). [PubMed: 22903516]

78. Mader S, Lutterotti A, Di Pauli F, Kuenz B, Schanda K, Aboul-Enein F, Khalil M, Storch MK, Jarius S, Kristoferitsch W, Berger T, Reindl M, Patterns of antibody binding to aquaporin-4 isoforms in neuromyelitis optica. PLOS ONE 5, e10455 (2010).

79. Mader S, Gredler V, Schanda K, Rostasy K, Dujmovic I, Pfaller K, Lutterotti A, Jarius S, Di Pauli F, Kuenz B, Ehling R, Hegen H, Deisenhammer F, Aboul-Enein F, Storch MK, Koson P, Drulovic J, Kristoferitsch W, Berger T, Reindl M, Complement activating antibodies to myelin oligodendrocyte glycoprotein in neuromyelitis optica and related disorders. J. Neuroinflammation 8, 184 (2011). [PubMed: 22204662]

80. Ruseva MM, Ramaglia V, Morgan BP, Harris CL, An anticomplement agent that homes to the damaged brain and promotes recovery after traumatic brain injury in mice. Proc. Natl. Acad. Sci. U.S.A 112, 14319–14324 (2015). [PubMed: 26578778]

81. Schiffer WK, Mirrione MM, Dewey SL, Optimizing experimental protocols for quantitative behavioral imaging with 18F-FDG in rodents. J. Nucl. Med 48, 277–287 (2007). [PubMed: 17268026]

82. Sawiak SJ, Wood NI, Williams GB, Morton AJ, Carpenter TA, Use of magnetic resonance imaging for anatomical phenotyping of the R6/2 mouse model of Huntington's disease. Neurobiol. Dis 33, 12–19 (2009). [PubMed: 18930823]

83. Rogers DC, Fisher EM, Brown SD, Peters J, Hunter AJ, Martin JE, Behavioral and functional analysis of mouse phenotype: SHIRPA, a proposed protocol for comprehensive phenotype assessment. Mamm. Genome 8, 711–713 (1997). [PubMed: 9321461]

84. Chavan SS, Huerta PT, Robbiati S, Valdes-Ferrer SI, Ochani M, Dancho M, Frankfurt M, Volpe BT, Tracey KJ, Diamond B, HMGB1 mediates cognitive impairment in sepsis survivors. Mol. Med 18, 930–937 (2012). [PubMed: 22634723]

85. Yang M, Crawley JN, Simple behavioral assessment of mouse olfaction. Curr. Protoc. Neurosci Chapter 8, Unit 8.24 (2009).

86. Chang EH, Volpe BT, Mackay M, Aranow C, Watson P, Kowal C, Storbeck J, Mattis P, Berlin R, Chen H, Mader S, Huerta TS, Huerta PT, Diamond B, Selective impairment of spatial cognition

caused by autoantibodies to the N-methyl-d-aspartate receptor. EBioMedicine 2, 755–764 (2015). [PubMed: 26286205]

87. Nestor J, Arinuma Y, Huerta TS, Kowal C, Nasiri E, Kello N, Fujieda Y, Bialas A, Hammond T, Sriram U, Stevens B, Huerta PT, Volpe BT, Diamond B, Lupus antibodies induce behavioral changes mediated by microglia and blocked by ACE inhibitors. J. Exp. Med 215, 2554–2566 (2018). [PubMed: 30185634]
88. Kowal C, DeGiorgio LA, Nakaoka T, Hetherington H, Huerta PT, Diamond B, Volpe BT, Cognition and immunity; antibody impairs memory. Immunity 21, 179–188 (2004). [PubMed: 15308099]
89. Ma Y, Hof PR, Grant SC, Blackband SJ, Bennett R, Slatest L, McGuigan MD, Benveniste H, A three-dimensional digital atlas database of the adult C57BL/6J mouse brain by magnetic resonance microscopy. Neuroscience 135, 1203–1215 (2005). [PubMed: 16165303]
90. Chang EH, Huerta PT, Neurophysiological correlates of object recognition in the dorsal subiculum. Front. Behav. Neurosci 6, 46 (2012). [PubMed: 22833721]
91. Tsien JZ, Huerta PT, Tonegawa S, The essential role of hippocampal CA1 NMDA receptor-dependent synaptic plasticity in spatial memory. Cell 87, 1327–1338 (1996). [PubMed: 8980238]
92. Sankowski R, Huerta TS, Kalra R, Klein TJ, Strohl JJ, Al-Abed Y, Robbiati S, Huerta PT, Large-scale validation of the paddling pool task in the clockmaze for studying hippocampus-based spatial cognition in mice. Front. Behav. Neurosci 13, 121 (2019). [PubMed: 31231197]

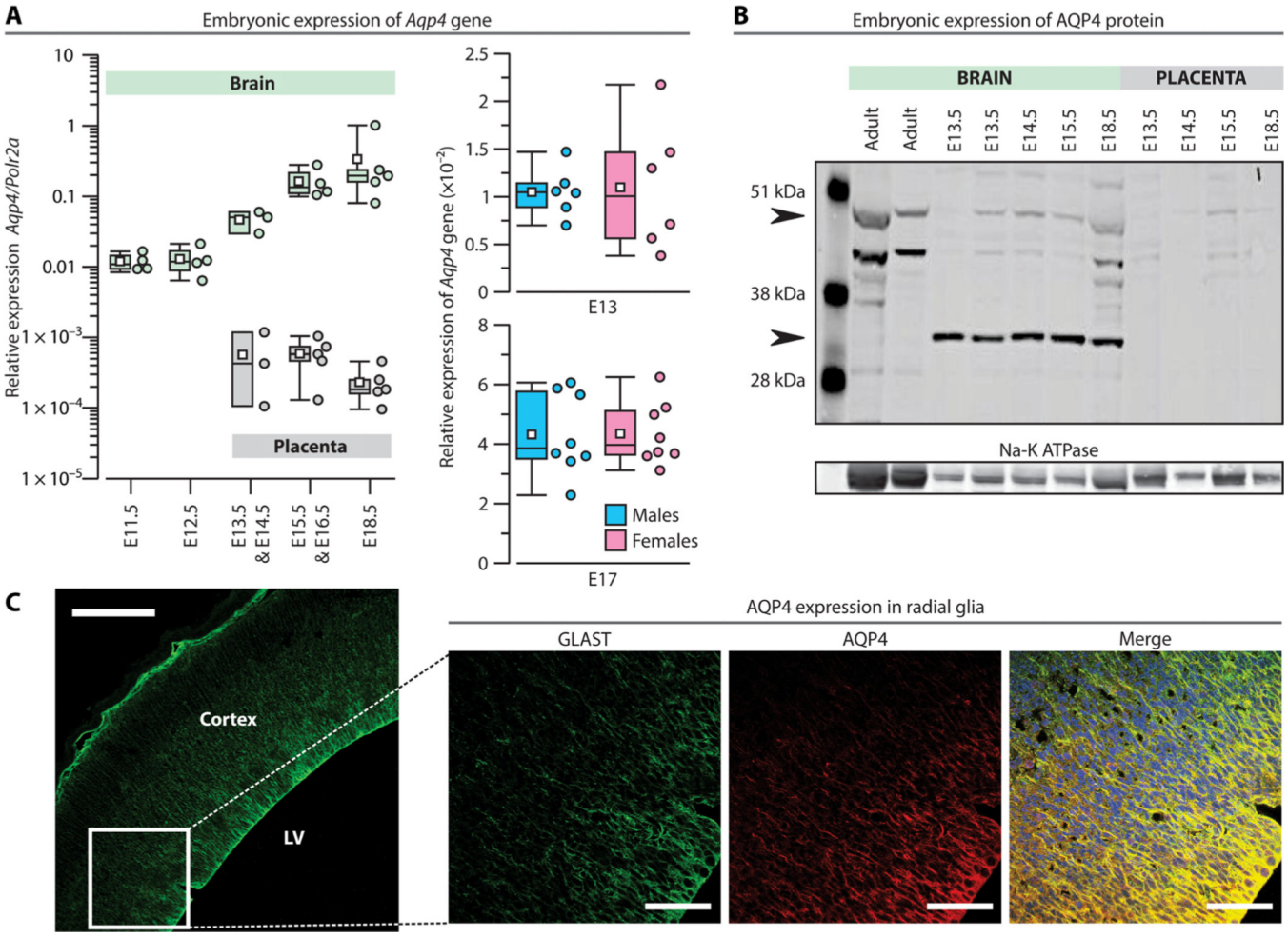

Fig. 1. The expression of AQP4 in the fetal mouse brain.

(**A**) Left: *Aqp4*-gene expression (relative to *Polr2A*) across embryonic days, in brain and placenta (box-and-whisker plot; brain at E11.5, $n = 4$; brain at E12.5, $n = 4$; brain at E13.5, $n = 3$; brain at E15.5, $n = 4$; brain at E18.5, $n = 5$; placenta at E13.5, $n = 3$; placenta at E15.5, $n = 5$; placenta at E18.5, $n = 5$). Right: *Aqp4*-gene expression in brain at E13 (top, six male and six female) and E17 (bottom, eight male and eight female). (**B**) Brain and placenta were analyzed for AQP4 expression by Western blot. Upper arrowhead points to adult (50 kDa) and lower arrowhead points to embryonic AQP4 (32 kDa) (representative of three experiments). Na-K ATPase (sodium–potassium adenosine triphosphatase) was used as loading control. (**C**) Left: Coronal section of cerebral cortex (E15.5) stained with anti-GLAST antibody (green) and anti-AQP4 (red). Boxed area corresponds to magnified sections (at right); LV, lateral ventricle. Right: Merge image showing colocalization of AQP4-signal with $GLAST^+$ RGCs (yellow). DAPI-stained nuclei are in blue (representative of three experiments). Scale bars, 250 μm (left) and 25 μm (right).

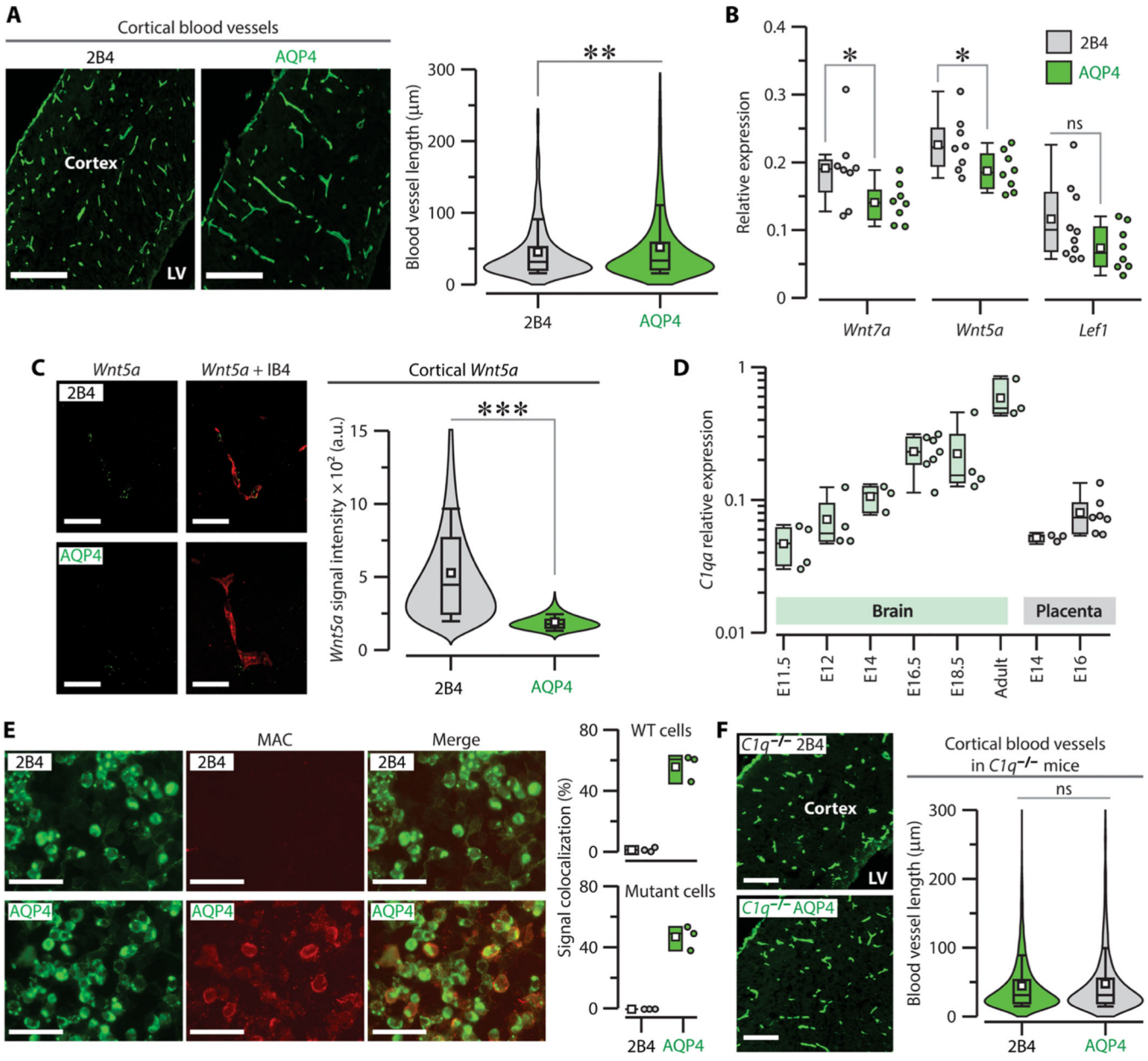

Fig. 2. Maternal AQP4-IgG causes abnormal vasculature in the fetal brain.

(**A**) Left: Representative cortical sections stained with isolectin-IB4 for blood vessels. Right: Violin plots show length of vessels, at E18.5, in AQP4 males [n = 2238 vessel segments (VS), six mice, range: 108 to 245 VS per animal] compared to 2B4 males (n = 2221 VS, six mice, range: 102 to 279 VS per animal); **P = 0.005, Kolmogorov-Smirnov (KS) test. (**B**) Box-and-whisker plot shows relative expression of WNT signaling genes (*P = 0.03 for *Wnt7*a, *P = 0.04 for *Wnt*5a, and P = 0.08 for *Lef*1, Student's t test). The cortex was extracted from AQP4 and 2B4 males (n = 8 mice, 2 liters, for each group), at P0; gene expression was measured by qPCR and normalized to *Polr*2A. (**C**) Left: Representative images of cortical blood vessels (Ib4, red signal) and *Wnt*5a RNA expression (green signal). Right: Violin plots show cortical *Wnt*5a signal intensity near the AQP4 vessels at E18.5

(2B4 males, $n = 114$, four mice, AQP4 males, $n = 120$, four mice; $^{**}P = 1.2 \times 10^{-25}$, KS test). a.u., arbitrary units. (**D**) Box-and-whisker plot shows *C1qa* transcript expression (relative to *Polr2A*) in the developing brain (E11.5, $n = 4$; E12, $n = 4$; E14, $n = 3$; E16.5, $n = 7$; E18.5, $n = 5$; adult, $n = 3$) and in the placenta (E14, $n = 3$; E16, $n = 7$) of untreated C57BL/6 mice. (**E**) Left: Mouse MAC formation (red signal) was analyzed in HEK cells expressing the nonglycosylated AQP4-fused with green fluorescent protein (GFP) (green signal, left) in the presence of the monoclonal AQP4-IgG or 2B4-IgG and mouse serum (middle and right panels, representative of three experiments). Right: Box-and-whisker plot shows the percentage of colocalization. Mean (95% confidence interval): wild-type (WT) cells; 2B4 = 1.21 (−2.18 to 4.6), AQP4 = 55.7 (34 to 77.4). Mutant cells; 2B4 = 0 (0 to 0), AQP4 = 47.1 (27.27 to 66.93). (**F**) Left: Representative images of embryonic cortex stained with isolectin-IB4. Right: Violin plots for cortical blood vessels of $C1q^{-/-}$ males at E18.5 (2B4, $n = 1390$ VS, four mice, 206 to 276 VS per animal; AQP4, $n = 1407$ VS, 6 mice, 115 to 272 VS per animal); $C1q^{-/-}$ AQP4 and $C1q^{-/-}$ 2B4 males ($P = 0.71$, KS test). (A and F) LV, lateral ventricle; ns, not significant. Scale bars, 250 μm (A and F), 20 μm (C), and 50 μm (E).

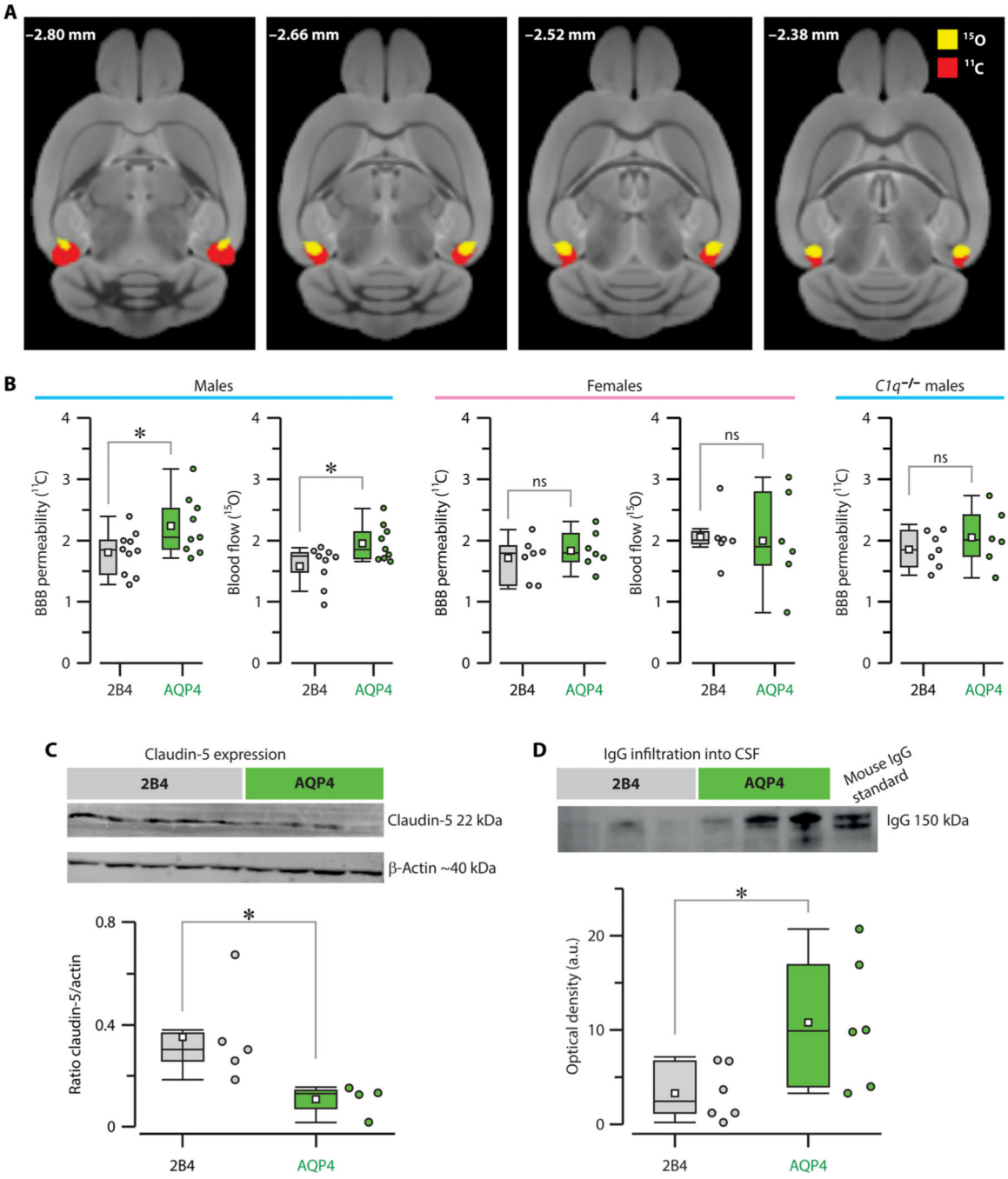

Fig. 3. MicroPET reveals impaired BBB in entorhinal cortex of adult AQP4 male mice.

(**A**) Voxel-wise search over the whole-brain volume shows a distinct region in which BBB permeability ([^{11}C]-AIB; red right cluster) and blood flow ([^{15}O]-H_2O; yellow right cluster) are increased at a threshold of $P < 0.001$ (voxel-level uncorrected) in AQP4 males compared to 2B4 males. The significant clusters from these two analyses are located in the right entorhinal cortex and overlap in this region. BBB permeability and blood flow values were measured post hoc in these clusters (right) and in the contralateral "mirror" regions (left) and averaged for the individual mice. (**B**) Box-and-whisker plots of mean BBB permeability and

blood flow in the bilateral entorhinal cortex. Left: Comparing between AQP4 and 2B4 males for BBB permeability (2B4, $n = 10$; AQP4, $n = 9$; $^*P = 0.036$, Student's t test) and blood flow (2B4, $n = 9$; AQP4, $n = 9$; $^*P = 0.023$, Student's t test). Middle: Comparing AQP4 and 2B4 females for changes in BBB permeability (2B4, $n = 7$; AQP4, $n = 7$) and blood flow [2B4, $n = 6$; AQP4, $n = 6$; ns, $P = 0.6$, Mann-Whitney U (MWU) test]. Right: Comparing BBB permeability in AQP4 and 2B4 $C1q^{-/-}$ males (2B4, $n = 7$; AQP4, $n = 6$; ns, $P = 0.5$, MWU test). (**C**) Top: Western blot shows claudin-5 protein expression in the cortex. Bottom, box-and-whisker plot shows claudin-5 expression (normalized to β-actin) in the AQP4 males compared to 2B4 males (2B4, $n = 5$; AQP4, $n = 4$; $^*P = 0.04$, MWU test). (**D**) Top: Western blot shows IgG in the CSF. Bottom: box-and-whisker plot shows the optical density of IgG in the CSF in AQP4 and 2B4 males (2B4, $n = 6$; AQP4, $n = 6$; $^*P = 0.02$, MWU test).

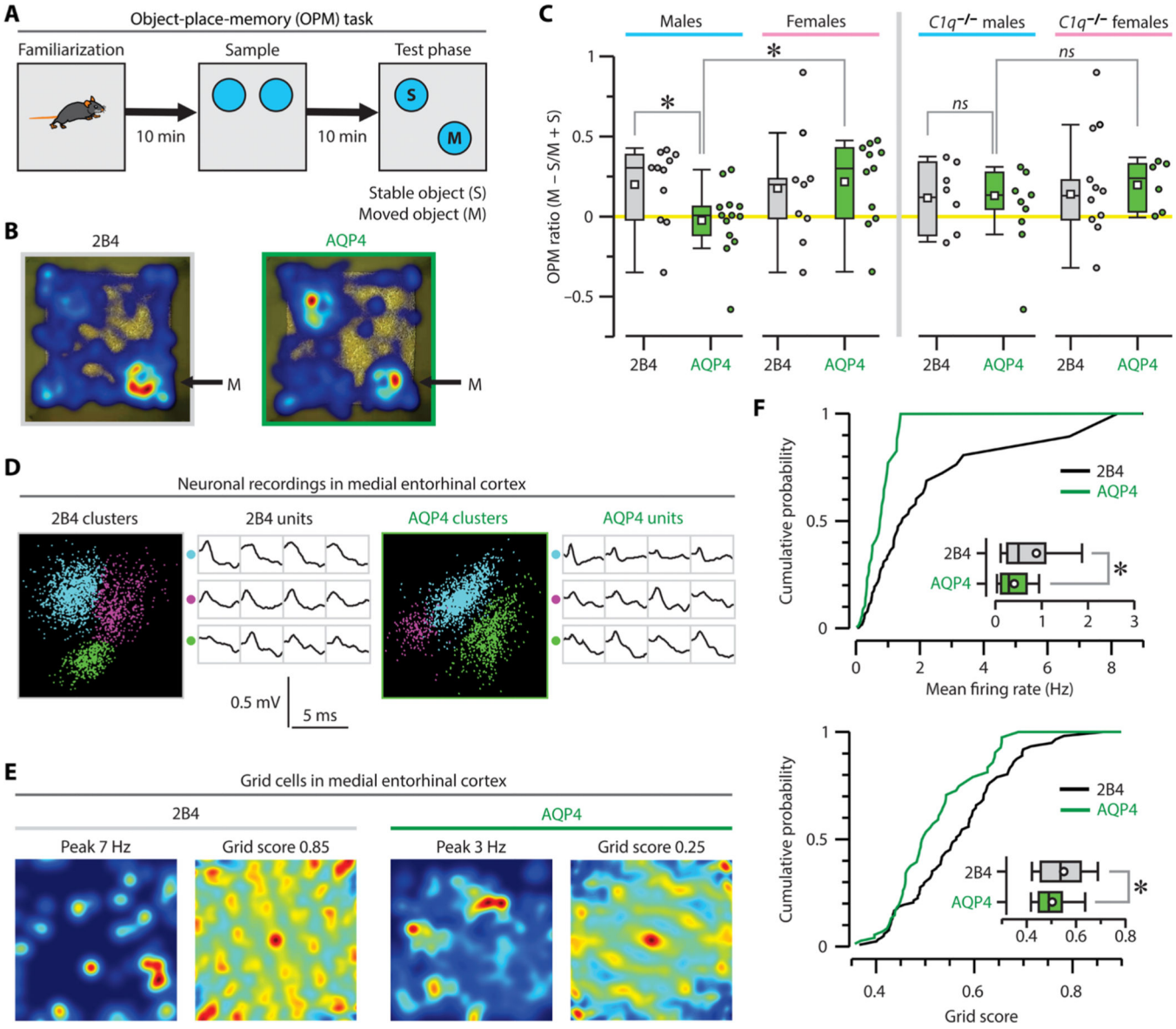

Fig. 4. Adult AQP4 male mice show impaired spatial cognition and disorganized entorhinal grid cells.

(**A**) Diagram of the OPM task. Each mouse is familiarized to the chamber and then exposed to two objects (sample phase, 5 min). For the test phase (5 min), one of the objects is moved to a different location. (**B**) Representative heatmaps of the test phase depicting the location of the nose of the mouse. 2B4 mice had a strong bias toward the moved object (M), which was lacking in AQP4 mice. (**C**) Box-and-whisker plots of OPM ratios (2B4 males, $n = 11$; AQP4 males, $n = 13$; 2B4 females, $n = 9$; AQP4 females, $n = 11$; $*P = 0.025$, AQP4 versus 2B4 males; $*P = 0.023$, AQP4 males versus AQP4 females; Student's t test). $C1q^{-/-}$ mice have normal OPM ratios for all groups (2B4 males, $n = 6$; AQP4 males, $n = 7$; 2B4 females, $n = 10$; AQP4 females, $n = 6$; ns, $P = 0.88$, AQP4-$C1q^{-/-}$ versus 2B4-$C1q^{-/-}$ males; ns, $P = 0.42$, AQP4-$C1q^{-/-}$ males versus AQP4-$C1q^{-/-}$ females; Student's t test). (**D**) Example cluster plots (left for each group) showing three simultaneously recorded neurons from a

tetrode. Colors allow visualization of each clustered unit. The waveforms (right for each group) are the action potentials in each channel of the tetrode. (**E**) Representative rate maps showing the firing rate of a single grid cell with respect to the location of the mouse (left for each group), and representative autocorrelation maps constructed from the displayed rate maps (right for AQP4 and 2B4 males). (**F**) Top: cumulative probability plot showing grid cell mean firing rates (2B4, $n = 87$ cells, four mice; AQP4, $n = 55$ cells, four mice; $*P = 0.0277$, KS test). Bottom: cumulative probability plot showing cell firing in AQP4 mice ($n = 55$) and 2B4 mice ($n = 87$), as calculated using the grid score metric; $*P = 0.0269$, KS test.

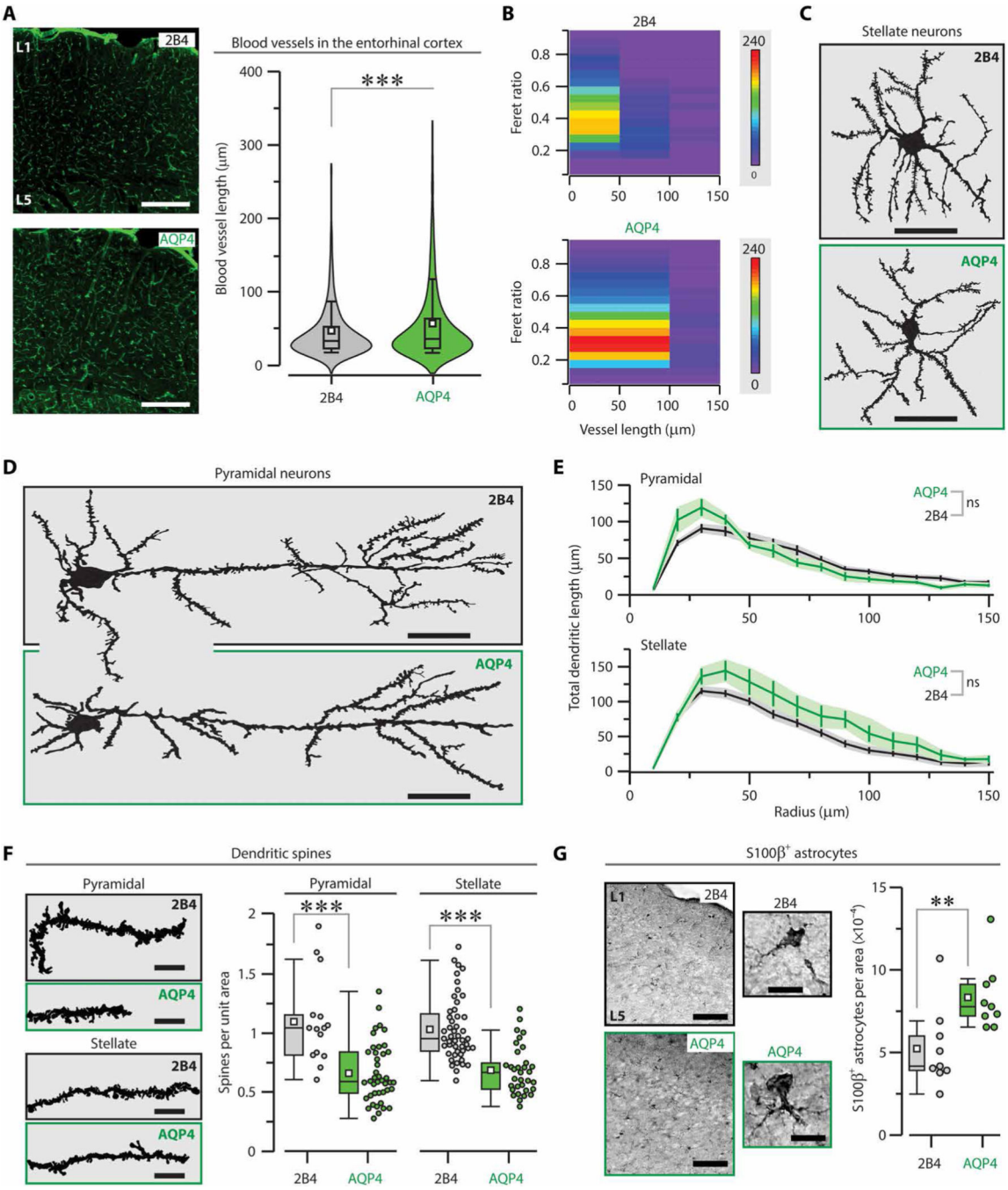

Fig. 5. Adult AQP4 male mice exhibit abnormal blood vessels and dendritic spines in the entorhinal neurons.

(**A**) Left: Representative sections were stained with lectin for blood vessels in the entorhinal cortex. Right: Violin plots show cortical vessel length in AQP4 males (n = 1898 VS, nine mice, range: 108 to 245 VS per animal) compared to 2B4 males (n = 1879 VS, eight mice, 102 to 279 VS per animal); ***$P = 3.5 \times 10^{-5}$, KS test. (**B**) Heatmap plots of vessel length in AQP4 male and 2B4 male mice (2B4, n = 1879 VS, eight mice; AQP4, n = 1898 VS, 9 mice; $P = 1.4 \times 10^{-9}$, KS test). The Feret ratio is calculated as F_{min}/F_{max}, where

F_{max} is the greatest width of the vessel contour and F_{min} is the least width; low ratios depict elongated objects, and values approaching 1 depict compact or circular objects. (**C**) Representative tracings of stellate neurons stained with Golgi method. (**D**) Example tracings of Golgi-stained pyramidal neurons. (**E**) Sholl analysis quantifies the total dendritic length (means ± SEM) in concentric rings (radius) from the cell body of pyramidal and stellate cells (2B4, $n = 49$ pyramidal, 59 stellate, four mice; AQP4, $n = 10$ pyramidal, 15 stellate, four mice; ns, $P = 0.4$, linear mixed model). (**F**) Analysis of dendritic spines (number of spines per unit area) in neurons of the entorhinal cortex in AQP4 and 2B4 males, for pyramidal cells (2B4, $n = 15$ dendrites, four mice; AQP4, $n = 42$ dendrites, four mice; ***$P = 0.00047$, Student's t test) and stellate cells (2B4, $n = 48$ dendrites, four mice; AQP4, $n = 33$ dendrites, four mice; ***$P = 6.4 \times 10^{-9}$, Student's t test). (**G**) Left: Sections show S100β-labeled astrocytes in the entorhinal cortex, with insets showing a magnified astrocytic cell. Right: Box-and-whisker plots show $S100\beta^+$ astrocytes per unit area in both groups of male mice (2B4, $n = 9$ sections, four mice; AQP4, $n = 9$ sections, four mice; **$P = 0.008$, MWU test). L1, layer 1; L5, layer 5. Scale bars, 500 μm (A), 20 μm (C), 20 μm (D), 5 μm (F), 500 μm (G), and 10 μm (G, inset).

Table 1.
Micro-PET brain analysis of adult AQP4 mice.

Values represent the means ± SD in the entorhinal cortex for FDG, ^{11}C, and ^{15}O injected to AQP4 and 2B4 mice. *P* values were calculated using Student's *t* test, two-tailed, with Welsch correction (equal variance not assumed). Whole-brain voxel-wise comparisons were done by analyzing across appropriate groups, on a voxel-by-voxel basis, and searching for any location with a significant difference. Preprocessed images have units in mCi (dose-corrected). Once brought into statistical parametric mapping (SPM), averaged images are ratio normalized by global mean.

Male	**FDG (*n* = 29)**	**^{11}C (*n* = 19)**	**^{15}O (*n* = 18)**
	17 2B4, 12 AQP4	**10 2B4, 9 AQP4**	**9 2B4, 9 AQP4**
2B4	1.93 ± 0.10	1.82 ± 0.35	1.59 ± 0.33
AQP4	1.91 ± 0.08	2.25 ± 0.48	1.96 ± 0.30
P [*t* value]	0.64 [0.47]	0.04 [2.27]	0.02 [2.51]
Female	**FDG (*n* = 15)**	**^{11}C (*n* = 14)**	**^{15}O (*n* = 12)**
	7 2B4, 8 AQP4	**7 2B4, 7 AQP4**	**6 2B4, 6 AQP4**
2B4	1.93 ± 0.03	1.71 ± 0.34	2.06 ± 0.45
AQP4	1.94 ± 0.06	1.84 ± 0.30	2.01 ± 0.81
P [*t* value]	0.9 [0.13]	0.46 [0.77]	0.90 [0.13]
***C1q*$^{-/-}$ Male**	**FDG (*n* = 13)**	**^{11}C (*n* = 13)**	
	7 2B4, 6 AQP4	**7 2B4, 6 AQP4**	
2B4	1.97 ± 0.09	1.85 ± 0.29	
AQP4	1.96 ± 0.15	2.05 ± 0.47	
P [*t* value]	0.98 [0.02]	0.37 [0.89]	

Table 2.

Micro-PET analysis of CSF in adult AQP4 mice

Percent change in CSF volume (means ± SD) calculated from FDG scans from AQP4 and 2B4 groups. *P* values were calculated using Student's *t* test.

Male	**2B4 (*n* = 17)**	**AQP4 (*n* = 12)**	***P* value**
Left	2.26% ± 0.17%	2.41% ± 0.23%	0.065
Right	2.33% ± 0.09%	2.43% ± 0.13%	0.018
Left and right	4.59% ± 0.23%	4.84% ± 0.34%	0.027
Female	**2B4 (*n* = 7)**	**AQP4 (*n* = 8)**	***P* value**
Left	2.46% ± 0.10%	2.38% ± 0.20%	0.31
Right	2.44% ± 0.09%	2.54% ± 0.11%	0.09
Left and right	4.91% ± 0.14%	4.92% ± 0.24%	0.92

Table 3.
Level of anti-AQP4 antibodies in serum of patients with NMOSD.

We used a cell-based assay to measure binding of NMOSD patient antibodies in serum to wild-type AQP4 (glycosylated) and to AQP4-containing mutations in the two glycosylation sites (nonglycosylated AQP4). We determined the highest dilution (titer) that still bound transfected cells. Antibody titers are shown as median (range, minimum to maximum) of patients showing no difference in binding (defined as a maximum of one titer level difference) compared to patients showing a difference in binding (defined as more than two titer levels difference) to glycosylated AQP4 and nonglycosylated AQP4. Age, sex, and gender or ethnicity for all study participants are included in data file S1.

	Patients with no difference in AQP4-IgG binding	Patients showing less binding to AQP4 nonglycosylated
Number	26/38 (69%)	12/38 (31%)
Glycosylated AQP4 titer	1280 (20–20,480)	1600 (40–20,480)
Nonglycosylated AQP4 titer	1280 (20–10,240)	240 (0–5120)